

Biphonon in the Klein-Gordon lattice

Laurent Proville

Service de Recherches de Métallurgie Physique,

CEA/DEN/DMN Saclay 91191-Gif-sur-Yvette Cedex, France

(Dated: February 19, 2019)

Abstract

A numerical approach is proposed for computing the nonlinear phonon excitations in a quantum Klein-Gordon lattice. In agreement with other studies^{1,2} on a different quantum lattice, nonlinearity is found to involve a phonon pairing and consequently some biphonon excitations. The energy branch and the correlation properties of the Klein-Gordon biphonon are studied in details.

PACS numbers: 63.20.Ry, 03.65.Ge, 11.10.Lm, 63.20.Dj

I. INTRODUCTION

In lattices made of identical particles or molecules, the energy is formulated by the Hamiltonian operator:

$$H = \sum_l \frac{p_l^2}{2m} + V(x_l) + \sum_{j=\langle l \rangle} W(x_l - x_j). \quad (1)$$

where x_l and p_l are displacement and momentum of the particle at site l , in a d -dimensional lattice. From the left to the right hand side of the equation Eq. 1, the energy contributions are identified as the kinetic energy, the local potential and the interaction between particles. That model is usually named Klein-Gordon lattice and our purpose is to study the case of quantum particles that are weakly interacting, i.e., the onsite energy V dominates the interaction W . For small amplitudes of displacements, the well-known harmonic approximation reduces H to a sum of quadratic terms, so the Shrödinger equation can be solved analytically. The elementary excitation is a plan wave which name is *optical phonon* and energy is fixed by the wave momentum q , in the lattice Brillouin zone. A consequence of the ideal harmonicity is that higher order excitations are simply the linear superpositions of these optical phonons.

For larger displacements, some non-quadratic contributions are involved in the expansion of H . Those terms usually refer to nonlinearity because they yield some forces that are not proportional to displacements. Then the Hamiltonian can no longer be diagonalized analytically. In a nonlinear KG lattice, F. Bogani³ derived some one- and two- phonon renormalized Green functions and showed that the nonlinear terms involve a pairing of the optical phonon modes. It confirmed the existence of biphonon excitations, studied earlier in a different lattice model by V.M. Agranovich⁴. A convincing agreement was found between theory³ and experiments⁵ in molecular crystals where the internal molecule bonds yield a strong nonlinearity.

The direct diagonalization of a KG Hamiltonian is, in principle, more precise than the computation of Green functions since it requires fewer approximations. In Ref. 6, by treating numerically the KG model, A. R. Bishop *and al.* confirm the existence of phonon bound states. Furthermore, some of these states have been shown to feature a particle-like energy band, for certain model parameters. The authors identified these specific excitations as being some quantum breathers (see Refs. 2,7,8,9,10 for more details about quantum breathers) because of their counterparts in classical mechanics^{11,12}. Nonetheless, the approach proposed

in Ref. 6 requires a huge computing cost so the size of lattices was limited to a one-dimensional (1D) chain of 8 unit cells. Moreover, the numerical simulations were restricted to the parameter region where the non-harmonic part of the lattice energy is modelled by a quartic onsite potential, i.e., the well-known ϕ^4 model. Our study may be thought as the continuation of Bishop's investigation⁶.

In the present paper, our numerical work tackles the d-dimensional quantum KG lattice with different forms of nonlinearity. The main advantage that offers our method is to analyze large enough lattice size to approach the infinite system features. When nonlinearity is significant, a pairing of phonon states is yielded and the so-called biphonon¹ branch contributes to the energy-spectrum. That branch splits from the two-phonon band by opening a gap. The width of that gap indicates the magnitude of nonlinearity since the biphonon gap vanishes completely for a pure harmonic lattice. In between the two extremes, i.e., harmonic and strongly nonlinear, the binding energy of the biphonon drops to zero at the center of the lattice Brillouin zone (BZ) while at the edge, the biphonon excitations are still bound. Then, in the energy-spectrum, the biphonon gap vanishes at the center, whereas a pseudogap is found to open at the edge of lattice Brillouin zone. We prove that it is a systematic feature of lattices in which nonlinearity is moderate. Similar results are obtained for the triphonon excitations.

Furthermore, we enhance how quantum properties of the biphonon depends on the form of nonlinearity. When the biphonon gap opens, the Klein-Gordon biphonon excitations show a finite correlation length, for all momentum q , on the condition that the non-quadratic energy term is a Φ^4 potential. That agrees with findings of Ref. 6. Considering the cubic term in the potential energy V , it is proved to involve a long range correlation of the biphonon states. The space correlation properties of triphonon are also studied and our results are used to establish some reasonable expectations on the existence of breather-like excitations in the quantum KG lattice.

The present paper is organized as follows. In Sec. II the model for the nonlinear discrete lattice is introduced and the computing method is detailed. Then it is tested for the quadratic lattices as well as for the ϕ^4 model. In Sec. III our results are presented concerning the biphonon spectrum while in Sec. IV the space correlation properties of the phonon bound states are studied. Finally, these results are discussed in Sec. V.

II. MODEL AND COMPUTING METHOD

A standard model for studying the nonlinear discrete lattices is the Klein-Gordon Hamiltonian, Eq. 1. At node i of a translational invariant d -dimensional lattice, the quantum particles of mass m evolve in a local potential V , each of them being coupled to its nearest neighbors, j by the interaction W . For moderate amplitudes of mass displacements around equilibrium, V and W can be expanded as Taylor series. The expansion of V is truncated to the fourth order:

$$V(x_i) = a_2 x_i^2 + a_3 x_i^3 + a_4 x_i^4 \quad (2)$$

while for W , only the quadratic terms is retained, i.e., $W(x_i - x_j) = -c(x_i - x_j)^2$. Higher order terms can be treated with no difficulty in our numerical method. Actually, they are found not to change our results qualitatively, at least for reasonable values of their energy coefficients that are consistent with optical modes.

Introducing the unitless operators $P_i = p_i/\sqrt{m\hbar\Omega}$, $X_i = x_i\sqrt{m\Omega/\hbar}$ where the frequency $\Omega = \sqrt{2(a_2 - 2.c.d)/m}$ is defined for either a chain $d = 1$ or a square lattice $d = 2$ or else a cubic crystal $d = 3$, the Hamiltonian reads

$$H = \hbar\Omega \sum_i \frac{P_i^2}{2} + \frac{X_i^2}{2} + A_3 X_i^3 + A_4 X_i^4 + \frac{C}{2} X_i \cdot \sum_{j=<i>} X_j \quad (3)$$

One finds the unitless coefficients:

$$A_3 = a_3 \sqrt{\frac{\hbar}{m^3 \Omega^5}}, \quad A_4 = a_4 \frac{\hbar}{m^2 \Omega^3} \quad \text{and} \quad C = \frac{4c}{m\Omega^2}. \quad (4)$$

For the harmonic lattice, i.e., $A_3 = 0$ and $A_4 = 0$, the Fourier transform of both the displacements and the momenta simplifies H into a sum of independent Hamiltonian:

$$h_q = \hbar\Omega \left(\frac{P_q^2}{2} + \frac{\omega_q^2}{2} u_q^2 \right) \quad (5)$$

with $\omega_q = \sqrt{1 - 2C \sum_k \cos(q_k)}$ and where q_k is the unitless coordinate of the wave vector in the k^{th} direction of the lattice. The periodic boundary conditions fixe $q_k = 2\pi l_k/L_k$ where L_k is the cells number in the k^{th} direction and l_k is an integer $l_k \in [1, L_k]$. Hence, using the standard harmonic oscillator theory, one finds the eigenvalues:

$$\Lambda_{\{n_q\}} = \hbar\Omega \sum_q \left(n_q + \frac{1}{2} \right) \sqrt{1 + 2C \sum_k \cos(q_k)} \quad (6)$$

where the n_q 's are the quanta number that take integer values from 0 to infinity and that fixe the energy contribution of the mode q . The eigenvalue $\Lambda_{\{n_q\}}$ is wholly determined by the set of integers $\{n_q\}$.

For the nonlinear case, the aforementioned procedure is no longer simple because non-quadratic terms, i.e., $(A_3u_i^3 + A_4u_i^4)$ yield a non-trivial coupling between the h_q operators. Thus we proceed differently, as described now. Starting from the exact diagonalization of the Hamiltonian where no interaction couples displacements, the low energy states are used to construct a set of Bloch waves upon which is expanded the entire Hamiltonian, including coupling W . The Shrödinger equation is then approximately solved with an error which shrinks to zero by increasing the basis cutoff.

The starting point is thus the eigenvalue problem for a single oscillator h_i :

$$h_i = \hbar\Omega\left(\frac{P_i^2}{2} + \frac{X_i^2}{2} + A_3X_i^3 + A_4X_i^4\right). \quad (7)$$

The Bose-Einstein operators $a_i^+ = \sqrt{2}(P_i + X_i)$ and $a_i = \sqrt{2}(X_i - P_i)$ are introduced in the writing of h_i :

$$\begin{aligned} h_i = & \hbar\Omega\left[a_i^+a_i + \frac{1}{2} + \frac{A_3}{\sqrt{8}}(a_i^{+3} + a_i^3 + 3a_i^+a_i^2 + 3a_i^{+2}a_i + 3a_i^+ + 3a_i) \right. \\ & \left. + \frac{A_4}{4}(a_i^{+4} + a_i^4 + 4a_i^{+3}a_i + 4a_i^+a_i^3 + 6(a_i^{+2}a_i^2 + a_i^{+2} + a_i^2 + 2a_i^+a_i) + 3)\right]. \end{aligned} \quad (8)$$

Expanding the operator h_i on the Einstein states, i.e., $|n, i\rangle = \frac{1}{\sqrt{n!}}a_i^{+n}|\emptyset_i\rangle$ for all $n \in \{0 \dots N-1\}$ gives a matrix \mathcal{M} of rank N . In each row of \mathcal{M} , one finds the nonzero coefficients:

$$\begin{aligned} \mathcal{M}_{n,n} &= \frac{3}{2}A_4n^2 + n(3A_4 + 1) + \frac{3}{4}A_4 + \frac{1}{2} \\ \mathcal{M}_{n,n+4} &= \frac{1}{4}A_4\sqrt{(n+4)(n+3)(n+2)(n+1)} \\ \mathcal{M}_{n,n+3} &= \frac{1}{\sqrt{8}}A_3\sqrt{(n+3)(n+2)(n+1)} \\ \mathcal{M}_{n,n+1} &= \frac{3}{\sqrt{8}}A_3\sqrt{(n+1)^3} \\ \mathcal{M}_{n,n+2} &= \frac{1}{4}A_4(4n+6)\sqrt{(n+2)(n+1)}. \end{aligned} \quad (9)$$

When the cutoff N tends to infinity, the Einstein states form a basis in the space of onsite states. The Shrödinger problem for the Hamiltonian h_i is thus equivalent to the diagonalization of \mathcal{M} . That diagonalization is compared to the semi-classical quantization¹³ in Fig. 1(a), for the case of a *He* atom embedded into a double-well potential: $V(x) = 16E_d/b^4x^2(x-b)^2$. The parameters, E_d and b , are the energy barrier and distance between minima, respectively (see Ref. 14). The very good agreement proves the efficiency of the diagonalization method even for a non-monotonous onsite potential. As shown in Fig. 1(b), each eigenvalue of \mathcal{M} is proved to converge to a steady value as N increases. In what follows, N is fixed large enough ($N = 500$) to compute the low energy eigenstates to machine precision. Arranging the onsite eigenstates by increasing order of their eigenvalues, the α^{th} eigenstate is denoted $\phi_{\alpha,i}$ and its eigenvalue is $\gamma(\alpha)$. In Fig. 2, for different sets of coefficients A_3 and A_4 , the bracket of the displacement operator, $\langle \phi_{\alpha,i} | X_i | \phi_{0,i} \rangle$, is plotted versus the rank α of $\phi_{\alpha,i}$. For further discussions (in Sec. IV), it is noteworthy that the absolute value of this bracket is maximum at $\alpha = 1$ and drops to zero with increasing α . In addition, $\langle \phi_{\alpha,i} | X_i | \phi_{0,i} \rangle$ takes zero value only for even α 's, provided that $A_3 = 0$.

We now treat the lattice in which atoms are interacting. Denoting i the S sites of the lattice ($S = \prod_{k=1}^d L_k$), the onsite state products $\Pi_i \phi_{\alpha_i,i}$ form a complete orthogonal base for the lattice excitations. In order to reduce the computer memory requirement, one takes advantage of the translation invariancy by introducing the Bloch wave formulation for the state products. Among those states some equivalent classes can be constructed in which each state results of a translation applied to an other state of same class. Retaining only one element for each translation class, the state which represents the class is identified by the series of its α_i 's, that is denoted $[\Pi_i \alpha_i]$. The construction of the equivalent classes is performed numerically. For each class, a Bloch wave can be written as follows:

$$B_{[\Pi_i \alpha_i]}(q) = \frac{1}{\sqrt{A_{[\Pi_i \alpha_i]}}} \sum_j e^{-iq \cdot j} \Pi_i \phi_{\alpha_i, i+j} \quad (10)$$

where $A_{[\Pi_i \alpha_i]}$ insures the normalization. Some attention must be payed to the possible translation symmetry of the state products that may be higher than the lattice symmetry. Indeed, for a given product there may be a lattice vector t that verifies $\Pi_i \phi_{\alpha_i, i} = \Pi_i \phi_{\alpha_i, i-t}$ with coordinates t_k such as $t_k < L_k$. It implies that $A_{[\Pi_i \alpha_i]} = S \cdot \prod_{k=1}^d (L_k/t_k - \text{fc}(L_k/t_k))$

where $fc(L_k/t_k)$ is the fractional portion of the ratio L_k/t_k . Then the Bloch wave can only takes the momentum q such as $q_k = 2\pi p_k/L_k = 2\pi p'_k/t_k$ where p_k and p'_k are some different integers.

The set of states $\{B_{[\Pi_i \alpha_i]}(q)\}_{q, N_{cut}}$, including the uniform state $\Pi_i \phi_{0,i}$ at $q = 0$, form a truncated basis where N_{cut} fixes the upper boundary on the onsite excitations, such as $\sum_i \alpha_i \leq N_{cut}$. When C is negligible, these states are the eigenstates of $H = H_0$. For moderate values of C , they should be some good approximates. As seen previously, for the single site problem, the truncation of the basis with a high enough cutoff may be expected not to affect the calculation of the low energy eigenstates. That assumption is verified for the harmonic lattice by comparing our calculations to the exact formula Eq. (6) (see Fig. 3 and below in the text for more details). As the study is focussed on the low energy excitations of large size lattices, the uniform states $\psi_\alpha = \Pi_i \phi_{\alpha,i}$ with $\alpha > 0$ are not considered into the calculation since the difference $\langle \psi_\alpha | H | \psi_\alpha \rangle - \langle \psi_0 | H | \psi_0 \rangle$ increases linearly with S (provided the groundstate of h_i is not degenerate).

Since the Bloch waves with different q are not hybridized by H , the Hamiltonian can be expanded severally with respect to q . It is performed analytically and gives a matrix $\mathcal{B}(q)$ the coefficients of which, are written as follows:

$$\begin{aligned} \langle B_{[\Pi_i \alpha_i]}(q) | H | B_{[\Pi_i \beta_i]}(q) \rangle = & \frac{1}{\sqrt{A_{[\Pi_i \alpha_i]} A_{[\Pi_i \beta_i]}}} [\Pi_i \delta_{\alpha_i, \beta_i} \sum_i \gamma(\alpha_i) - \frac{C}{2} \sum_{l,j} \exp(-iq \cdot j) \\ & \cdot \sum_{k=\langle l \rangle} sc(\alpha_l, \beta_{l+j}) \cdot sc(\alpha_{l+k}, \beta_{l+k+j}) \Pi_{i \neq l, l+k} \delta_{\alpha_i, \beta_{i+j}}] \end{aligned} \quad (11)$$

where $sc(\alpha_i, \beta_i)$ denotes the bracket $\langle \phi_{\alpha_i} | X_i | \phi_{\beta_i} \rangle$ that is given by:

$$sc(\alpha_i, \beta_i) = \frac{1}{\sqrt{2}} \sum_{l=0}^N \langle \phi_{\alpha,i} | l, i \rangle (\sqrt{l+1} \langle l+1, i | \phi_{\beta,i} \rangle + \sqrt{l} \langle l-1, i | \phi_{\beta,i} \rangle). \quad (12)$$

The eigenvalues of $\mathcal{B}(q)$ are computed numerically with an exact HouseHolder method¹⁵. The only value of N_{cut} fixes the precision of our calculation which can be compared with the analytical expression in Eq. (6), for a pure harmonic lattice. For a one-dimensional (1D) chain, that comparison is done in Fig. 3 where are reported our results for different N_{cut} . The insert in Fig. 3 shows the two-phonon energy region. The precision improves with increasing N_{cut} but the computing time increases too. So for the large size system the numerics are performed with $N_{cut} \leq 4$ in 1D whereas in 2D, $N_{cut} \leq 3$. It is noted that for achieving a fixed precision, the required N_{cut} increases with both parameter C and size S . It

is due to the terms $a_i^+ a_j^+$ or $a_i a_j$ that come from the realistic coupling W . These operators involve a quantum hybridization with some high energy Bloch waves that are neglected.

In Fig. 4, for a 1D chain with $S = 4$, our calculation is compared to Ref. 6. In Ref. 16, our model parameters are written as some functions of parameters defined in Ref. 6. A very good agreement is observed for the low energy states. In the present work, the lattices that can be treated have typical size $S = 33$ in 1D and $S = 13 \times 13$ in 2D. These performances could be improved again by computing the $\mathcal{B}(q)$ diagonalization with a non-exact numerical procedure which have not been done here.

III. GAP AND PSEUDOGAP IN THE OPTICAL PHONON SPECTRUM

For different values of nonlinear coefficients A_3 and A_4 , we first examine the vibration spectrum of a one-dimensional (1D) lattice. The 2D lattice is treated at the end of the present section.

When the non-quadratic part of the lattice energy is negligible, the eigen-spectrum of H is composed of the fundamental optical branch due to the phonon states (in Eq. 6, a single q verifies $n_q = 1$) and the branches due to the linear superpositions of these phonons (in Eq. 6, several q 's verify $n_q = 1$). The latest branches are staked together into distinct bundles, each of them filling in a compact range of energy. In Fig. 5 and following ones, each eigenvalue of the finite size Hamiltonian is reported as a single circle symbol. The distinct eigen-energies participate to different branches. The phonon branch is marked with the tag $\{1\}$ while the branches that are due to the linear superposition of two phonon states are pointed out by the tag $\{11\}$. For a macroscopic system, the bundle $\{11\}$ covers a dense range of energy and forms a continuous band. The width of an optical phonon branch being physically of a few percent of the elementary excitation energy, the unitless coupling C is fixed to $C = 0.05$ which gives indeed a phonon branch width $\Delta_1 \approx 10\%$ of the phonon energy (see left-hand inserts in Figs. 5-6).

When nonlinearity is significant, the parameters A_3 and A_4 are not negligible in Eq. (3). Then, as shown in the left-hand inserts in Figs. 5 (a) and 6 (a), the phonon branch shows no qualitative change in comparison with the fundamental optical branch of a harmonic lattice. However, an isolated spectral branch is found in addition to phonon branch and its combination tones (see Figs. 5(a) and 6(a) and magnifications in the right-hand inserts). In

Fig. 7, varying artificially the coupling C to the trivial case $C = 0$ demonstrates that the additional branch coincides with the energy of the Bloch wave $B_{[\alpha,0,\dots,0]}$ with a single onsite excitation $\alpha = 2$. In Fig. 5 and next ones, the additional branch is marked with a single tag $\{2\}$. By analogy with biphonon theory¹, that branch is identified as the energy of biphonon. Similar results are found for the triphonon states which branch is pointed by the tag $\{3\}$ in Fig. 7. The reason for these isolated branches is that onsite Hamiltonian eigenvalues $\gamma_{\alpha>1}$ do not match the linear fit given by $(\gamma_1 - \gamma_0)\alpha + \gamma_0$. This is the consequence of h_i anharmonicity. The differences $\gamma_{\alpha>1} - [(\gamma_1 - \gamma_0)\alpha + \gamma_0]$ results of the non-quadratic terms in the potential V (Eq. (3)). These differences involve some gaps in the $C = 0$ spectrum which is composed of energies of states $B_{[\Pi_i\alpha_i]}$. A moderate inter-site coupling hybridizes states $B_{[\Pi_i\alpha_i]}$ but largest gaps of the $C = 0$ spectrum remain (Fig. 7).

The raising of degeneracy of $B_{[\Pi_i\alpha_i]}$ where only 2 α_i 's equal 1 and the rest is zero (number of these states is $S(S-1)/2$ and their energy is $2\gamma(1) + (S-2)\gamma(0)$) yields a bundle of branch which energy corresponds to the linear superposition of two single phonon states. In Fig. 7, for higher energy, other bundles are pointed out by the tags $\{21\}$ and $\{111\}$. At zero coupling, these branches coincide with the energy of the states $B_{[2,1,0,\dots,0]}$ and $B_{[1,1,1,0,\dots,0]}$. For a macroscopic lattice, the bundles $\{21\}$ and $\{111\}$ contribute to the dense energy spectrum as well as $\{11\}$ and they form some bands. They can be thought as the unbound associations of a biphonon state with a single phonon state and the three-phonon states, respectively.

In Figs. 5(a) and 6(a), for different parameters, the biphonon branch splits from the two-phonon band. Measuring the energy of a biphonon state with reference to the unbound two-phonon for same momentum q , a binding energy of the biphonon is defined. A positive binding energy occurs when the onsite potential V is harder than a harmonic function (Fig. 5(a)) whereas a softening yields a negative binding energy (Fig. 6(a)). The biphonon energy gap is equal to the minimum of the absolute value of binding energy with respect to q . The biphonon gap reveals the strength of nonlinearity insofar as when the biphonon gap overpasses the phonon branch width (as it does in Figs. 5(a) and 6(a)), it clearly indicates a significant contribution of non-quadratic terms. While in Figs. 5(a) and 6(a), a biphonon gap opens, it is found that when nonlinearity is weak the biphonon binding energy vanishes at center of the lattice Brillouin zone (BZ) (Figs. 5(b) and 6(b)). However,

at the edge of BZ, the binding energy is comparable to the width of the phonon branch Δ_1 (inserts in Figs. 5(b) and 6(b)). Consequently, a pseudogap is yielded when non-quadratic energy has same magnitude as inter-site coupling. In this regime, the biphonon excitations exist only at the edge of BZ while they are dissociated into unbound phonon at center. With similar results, other calculations have been performed for different parameters. They showed that the biphonon pseudogap is a generic feature of lattices where nonlinearity is moderate. Moreover that pseudogap opens at the edge of BZ, even though the coupling sign is changed. For a very weak nonlinearity, the binding energy of the biphonon is negligible for all q but strictly speaking the pseudogap opens as soon as the nonlinear coefficients are non-zero. So it is the q -range where nonlinear behavior is likely to be experimentally measured in materials where nonlinearity is weak.

In Fig. 7, the low energy eigenvalues of H are plotted versus parameter C . The variations of the biphonon and the triphonon branches are pointed out by the tags $\{2\}$ and $\{3\}$, respectively. In a similar manner, there are represented the bands that correspond to unbound two-phonon states $\{11\}$, unbound three-phonon states $\{111\}$ and unbound states composed of the superposition of a single biphonon and a single phonon state $\{21\}$. It can be noted that the width of the phonon bound state branch increases with C much slower than unbound phonon bands. The branch of the α -phonon bound states (with $\alpha = 2$ or $\alpha = 3$) are found to merge with unbound phonon bands for a certain threshold C_α . At $C < C_\alpha$, the α^{th} branch and the unbound phonon bands are separated by a gap whereas around $C \approx C_\alpha$, only a pseudogap separates them partially. The C_α threshold depends on both coefficients A_3 and A_4 and it is different for each α -phonon bound state branch because of anharmonicity of h_i eigenvalues. A unique set of nonlinear parameters A_3 and A_4 corresponds to the energy distribution of the biphonon and triphonon branches. So in principle, if a spectroscopy is able to measure the biphonon and the triphonon resonances, it is sufficient for inverting our numerical treatment and thus determining the nonlinear parameters. Moreover, the results in Fig. 7 demonstrate that even though the non-quadratic terms in V are not large enough to open a biphonon gap, i.e., $C > C_2$ then a gap or at least a pseudogap opens for the α -phonon bound states with $\alpha > 2$. Eventually, the theoretical results in Fig. 7(b) are qualitatively very similar to the experimental findings of Ref. 17 in which the Raman analysis of the high pressure molecular H_2 shows a pressure-induced bound-unbound transition of the so called bivibron around 25 GPa. There is indeed a likeness between Fig. 10 in Ref. 17 and

the two-phonon energy region in Fig. 7 (b). In the framework of our model, the pressure variation of experiments¹⁷ can be simulated by a change of the coupling parameter C due to the fact that first atom neighbors are moved closer together because of the external pressure. Actually, the increase of C induces a bound-unbound transition of the biphonon at $C = C_2$. When following our thought process, the experimental determination of C_α (with $\alpha = 2$ or $\alpha = 3$), as performed in Ref. 17 for $\alpha = 2$, can allow to quantify precisely the nonlinear coefficients A_3 and A_4 and thus to characterize precisely the potential landscape of quantum particles. For that purpose, it is required to fit the spectroscopy data with the numerical treatment that is proposed here.

In Fig. 8, the diagonalization of a two-dimensional (2D) lattice Hamiltonian is performed for $A_3 = 0$ and for different values of A_4 . The coupling amplitude is such as the phonon band width Δ_1 is a few percent of the elementary excitation branch. By estimating that $\Delta_1 \approx 2.d.|C|$, the value of the unitless coupling is fixed around $C = 0.025$. In the biphonon energy region, a gap opens when A_4 is large (top of Fig. 8) whereas that gap closes at the center of the lattice Brillouin zone when $A_4 = 0.025$ (bottom of Fig. 8). In the latter case, a pseudogap is found to open around $q = \pi[11]$ and the width of that pseudogap has same order of magnitude as the phonon band width. These both quantities can be compared in inserts of Fig. 8 that show the profile of the spectrum along the direction $[11]$ of the reciprocal lattice. The pseudogap width is same as in Fig. 5 for the 1D chain. Consequently, a pseudogap is expected for all lattice dimensions when both the inter-site coupling and the non-quadratic energy have a comparable magnitude.

IV. CORRELATION PROPERTIES OF THE MULTI-PHONON STATES

In the present section, the study is focussed on the space correlation of the multi-phonon states in a 1D lattice. The space correlation function for displacements is defined as follows:

$$f(\Phi, n) = \sum_l \langle \Phi | X_l X_{l+n} | \Phi \rangle - \langle \Phi | X_l | \Phi \rangle \langle \Phi | X_{l+n} | \Phi \rangle \quad (13)$$

where Φ is an eigenstate and n is the unitless distance ($n > 0$). For an harmonic lattice, $A_4 = 0$ and $A_3 = 0$, it is easily verified that $f(\Phi, n) = \sum_q \cos(q \cdot n)$ for a state Φ which is composed of the linear superposition of phonon states which q 's are the momenta. The single phonon correlation function is a simple $(\cos(q \cdot n))$. Then, the correlation functions

exhibit a space modulation with a constant amplitude. At $q = 0$, the function $f(\Phi, n)$ is a non-zero constant for all n .

Before describing our results, it is convenient to compute analytically the function $f(\Phi, n)$ for the Bloch waves $B_{[\Pi_i \alpha_i]}$ (Eq. 10) with only one onsite excitation of order α . These states writes:

$$B_{[\alpha, 0, \dots, 0]}(q) = \frac{1}{\sqrt{S}} \sum_j e^{-iq \cdot j} \phi_{\alpha, k+j} \cdot \prod_{l \neq k} \phi_{0, l+j}. \quad (14)$$

Let us introduce the notation, $\psi_\alpha(q)$ for these states. At the uncoupled limit ($C = 0$), the onsite excitation Bloch waves correspond to eigenstates of H (see Fig. 7 and text in Sec. III). The space correlation function of $\psi_\alpha(q)$ is given by:

$$f(\psi_\alpha(q), n) = 2sc(\alpha, 0)^2 \cos(q \cdot n) - \frac{(sc(\alpha, \alpha) - sc(0, 0))^2}{S} \quad (15)$$

where $sc(\alpha, 0) = \langle \phi_{\alpha_i} | X_i | \phi_{0_i} \rangle$ and $sc(\alpha, \alpha) = \langle \phi_{\alpha_i} | X_i | \phi_{\alpha_i} \rangle$ as indicated in Eq. 12. The constant term in the right hand side of Eq. 15 vanishes when the lattice size S increases. In the numerical computations that are presented below, for finite size lattices, that constant is removed in order to approach the behavior of the infinite size lattices. Another point which is noteworthy is that, in general, the displacement operators are correlated for a given state $\psi_\alpha(q)$. Indeed the bracket $sc(\alpha, 0)$ (plotted in Fig. 2 for different nonlinear parameters) is usually not zero and the function $f(\psi_\alpha(q), n)$ shows a space modulation of amplitude $R_\alpha = 2sc(\alpha, 0)^2$. Strictly speaking the bracket $sc(\alpha, 0)$ is zero only for even values of α on condition that $A_3 = 0$. The coefficients R_α are given in table Tab. I for parameters used in previous calculations (Figs. 5 and 6).

The function $f(\Phi, n)$ is plotted in Figs. 9-11 for eigenstates Φ that are either the phonon, biphonon or triphonon states. For each of these states, $f(\Phi, n)$ is computed for several values of q . The calculations at $C > 0$, demonstrate that the long range behavior of the correlation function for phonon states ($\alpha = 1$) as well as for α -phonon bound states ($1 < \alpha < 4$) is similar to the variations of the function $f(\psi_\alpha(q), n)$, i.e., the modulations have same amplitudes, fixed by R_α . This property holds provided that the α^{th} discrete branch is separated from the rest of energy spectrum by some gaps. In Figs. 9(a)-11(a), the correlation function of phonon states shows a modulation which extends over the whole lattice as in the pure harmonic lattice. For large n , the variations of $f(\Phi, n)$ are similar to ones of $f(\psi_1(q), n)$,

Eq. 15. Indeed the amplitude of the modulations is given by the coefficient R_1 (see Tab. I). The correlated character of the phonon states is thus related to the feature of the onsite excitation Bloch wave $\psi_1(q)$ and more precisely to the fact that the onsite displacement operator generates an overlap between the onsite groundstate $\phi_{0,i}$ and the first excited state $\phi_{1,i}$. The agreement between the long range behavior of phonon states and $\psi_1(q)$ holds in the harmonic lattice. That can be checked by comparing the exact formula $f(\Phi, n) = \cos(q n)$ for a single phonon state in the harmonic chain with the equation Eq.15, noting that for a quadratic form of V , we have $sc(1, 0) = 1/\sqrt{2}$.

The agreement between the coefficient R_α and the long range modulations of $f(\Phi, n)$ is not strictly proved for biphonon and triphonon (see Tab. I and Figs. 9(b-c) and 10(b-c)) because the corresponding branches are too close from the unbound phonon bands. Nevertheless we estimate that the agreement roughly holds. It can be noted in Figs. 9(b) and 10 (b) that it does indeed, whereas in Figs. 11(b) it does not because the biphonon gap closes for small q . Provided the α^{th} discrete branch is isolated in the energy spectrum, there is no conceptual difference between α -phonon bound states and phonon states because they all come from the raising of the translational degeneracy of the onsite eigenstates $\phi_{\alpha,i}$. Actually, we conclude that the coefficient R_α is a good indicant of long range correlations for the α -phonon bound states (including the phonon states with $\alpha = 1$) on the condition that their hybridization with other phonon states is negligible. Therefore, when $R_\alpha = 0$, the α -phonon bound states exhibit a finite correlation length provided the α^{th} discrete branch is isolated in the energy spectrum. In Fig. 9(b), the space correlation function vanishes for the large n and for all q as R_2 equals zero (see Tab.I).

As shown in Fig. 2 and Tab. I, $sc(\alpha, 0)$ and subsequently $R_\alpha = 2sc(\alpha, 0)^2$ drop to zero with increasing α . Above $\alpha = 4$, R_α may be consider as physically negligible. By extension of our results about space correlations of the α -phonon bound states with $\alpha < 4$, it is expected that the α -phonon bound states with $\alpha \geq 4$ have a finite correlation length provided their energy branch remains isolated from the linear combination bands of the lower energy states, i.e., from the unbound phonon states as well as from the combinations of the lower order multi-phonon bound states (for instance, see {21} in Fig. 7). For the specific case $A_3 = 0$ and $A_4 > 0$, the even values of α verify $R_\alpha = 0$, so the corresponding α -phonon bound states have also a finite correlation length when their branch is isolated in the spectrum. For a closing biphonon gap, a pseudogap was found to

persist at the edge of the lattice Brillouin zone (Sec. III). In Fig. 11(b), it is shown that the biphonon states have a finite length scale only for momenta in the BZ range where the pseudogap opens. Indeed, due to hybridization with the two-phonon states, the biphonon at $q \approx 0$ have a non-vanishing space correlation function which overpasses the finite lattice size.

The phonon bound states with a finite correlation length, exhibit a singular feature that is worth to characterize more precisely. For that purpose, let denote $\Phi_\alpha(q)$, the wave function of the α -phonon bound state with momentum q and $E_\alpha(q)$, the unitless energy of the α^{th} branch. One introduces the time dependent Wannier state $W_\alpha(t, n)$, which is constructed from a combination of the α -phonon bound states:

$$|W_\alpha(t, k) \rangle = \frac{1}{\sqrt{S}} \sum_q e^{-i(q \cdot k + E_\alpha(q)\Omega t)} |\Phi_\alpha(q) \rangle. \quad (16)$$

The subscript k indicates the lattice site where is centered the Wannier transform.

In Fig. 12, the plot of the scalar product $|\langle \psi_\alpha(q) | \Phi_\alpha(q) \rangle|$ is reported for $\alpha = \{1, 2, 3\}$. Keeping fixed $A_3 = 0$ and $C = 0.05$, the parameter A_4 is increased from zero. The scalar product $|\langle \psi_\alpha(q) | \Phi_\alpha(q) \rangle|$ is proved to equal 1 when the gaps that surround the α^{th} branch are large, or equivalently when A_4 is large. Then one can reasonably argue that the Bloch wave $\psi_\alpha(q)$ is a very good approximate of the α -phonon bound state and the corresponding eigen-energy is approached by:

$$\langle \psi_\alpha(q) | H | \psi_\alpha(q) \rangle = \gamma_\alpha + (S - 1)\gamma_0 - Cf(\psi_\alpha(q), 1). \quad (17)$$

When $A_3 = 0$, the correlation function $f(\psi_2, n)$ is zero for all n (since $R_2 = 0$, see Tab. I), so, for the biphonon, we obtain $E_2(q) = \gamma_2 + (S - 1)\gamma_0$. Then the energy $E_2(q)$ does not depend on q , $E_2(q) = E_2$, and the Wannier state $|W_2(t, k) \rangle$ can thus be rewritten as follows:

$$|W_2(t, k) \rangle = e^{-i(E_2\Omega t)} \phi_{2,k} \prod_{l \neq k} \phi_{0,l}. \quad (18)$$

It is obvious that such a state is a localized and time periodic excitation of the lattice. The classical counterparts of such state would be the breather solutions for the classical nonlinear discrete lattice, first enhanced by A. J. Sievers and S. Takeno¹¹. These classical breather solutions have two important features that are first their spacial localization and second their time periodicity with a frequency that is out of both the linear classical phonon

branch and its resultant harmonic bands (for an exact proof see Ref. 12). Our assumption about the classical counterparts could be justified by checking whether are comparable the energies of a localized time periodic Wannier state and the semi-classical quantization of the classical breather orbits, in same lattice.

Extending our sketch to all the α -phonon bound states, the conditions for a breather-like Wannier state in a KG lattice are twofold: first, the branch of the α -phonon bound states must be isolated by large surrounding gaps and second, $R_\alpha = 0$. Let us detail the breaking of these conditions. When the α^{th} branch is isolated but $R_\alpha > 0$, the $\psi_\alpha(q)$ are still some good approximates for the α -phonon bound states (see in Fig. 12 for the phonon and the triphonon). Then the band width of the α^{th} branch does not vanish because of the self-tunneling of ψ_α , i.e., the inter-site coupling hybridizes the Bloch wave $\psi_\alpha(q)$ with itself. The Wannier transform (Eq.16) of ψ_α is a combination of states, non-coherent in time, since $E_\alpha(q)$ depends on q . It is no longer a time-periodic solution. On the opposite, after a certain laps time Δt_c , the Bloch waves ψ_α do no longer interfere. This Δt_c is inversely proportional to Δ_α , that is the band width of the α^{th} branch. When $R_\alpha = 0$ but the α^{th} branch is not isolated, the Bloch wave ψ_α is hybridized with unbound phonon states. Then the Wannier state in Eq.16 is no longer strongly localized as the breather-like Wannier state in Eq.18, but it shows some spacial extensions. In addition, $E_\alpha(q)$ depends on q (as shown in Fig.5 (b), for the biphonon). Hence the Wannier transform is not coherent in time and $W_\alpha(t, k)$ is not time-periodic after the duration Δt_c .

Finally, we found that the localized and time periodic excitations exist in the quantum KG lattices that are strongly nonlinear.

V. PERSPECTIVES

In the present paper, the pairing of phonon states in the Klein-Gordon (KG) lattice has been considered with numerics. Since the KG Hamiltonian involves very few approximations, a realistic modelling of both quantum hybridization and pairing of phonon states has been achieved. The biphonon pseudogap has been proved to characterize lattices where nonlinearity is moderate. The quantum properties of biphonon were found to depend on the form of nonlinearity. In general, the KG biphonon exhibits some long range correlations as the phonon do. However in the specific case of a Φ^4 potential, the biphonon states

feature a finite correlation length. When nonlinearity plays a dominant role, according to our expectations, the tunneling of certain multi-phonon bound states vanishes which reveals some breather-like excitations.

The phonon bound states have been identified by infrared measurements in molecular crystals, as for N_2O or CO_2 . For such crystals, the internal molecule bonds involve a significant non-quadratic contribution to the energy. The corresponding nonlinear modes were revealed by some anharmonic resonances that are isolated in the absorption infrared spectrum. These resonances were analyzed successfully in the theoretical work of F. Bogani⁵. An extremely good agreement had been obtained in comparing the theoretical calculations to experiments on the molecular crystals. As F. Bogani used a KG model³, with some refinements on the internal molecular modes, we believe that similar results could be achieved within our numerical approach.

The debate about the spectral branch $\Delta'_2(\text{LO})$ of diamond (see Refs. 22,23 for the different points of view) showed that the interpretations of spectroscopy data may diverge when the magnitude of nonlinearity is not sufficient for yielding some isolated resonances out of the overtone regions. In the compounds where nonlinearity is not large enough to separate the spectral resonances of bound and unbound phonon states, it is required to analyze the pseudogaps of biphonon, triphonon or even higher order phonon bound states. For that purpose, it might be of experimental interest to calculate the dynamic structure factor $S(q, \omega)$ in lattices where a pseudogap opens, in order to identify the corresponding neutron scattering spectrum. The multi-phonon bound states with a finite correlation length have been shown to contribute to the $S(q, \omega)$ function with a specific signature⁶. The adjustment of KG parameters could permit to fit the spectroscopy data and thus to determine quantitatively the potential energy of quantum particles in compounds under investigation.

As for the molecular crystals N_2O or CO_2 , the adsorbed surface $\text{Ru}(100):\text{CO}$ shows a nonlinear CO stretching mode, according to its isolated anharmonic resonances in the infrared spectrum¹⁸. Changing the CO coverage, P. Jakob *et al.*¹⁸ observed a variation of the biphonon resonance. Several theoretical approaches have been recently attempted with different models^{18,19}. There is proposed a rescaling of internal anharmonicity of

CO molecule as a function of coverage. In order to analyze unambiguously the surfaces Ru(100):CO under the scope of a KG model, some more experimental data would be needed on the triphonon resonance so as to determine the polynomial series of the local potential V .

Another type of nonlinear lattice have been studied extensively in literature. In the early seventies, V.M. Agranovich (for a review, see Ref. 1) introduced a qualitative approach where some effective boson quasi-particles model the molecule's vibrations. The purpose was then to propose a theoretical tool which could be handled analytically, on the opposite to the KG lattice. There, the nonlinear lattice behavior is simulated by a onsite Hubbard interaction between the boson pairs. Recently, that effective Hubbard Hamiltonian for boson has regained some interest with different extensions²⁰. The eigenvalue problem for two bosons can be expressed as a Discrete Non-Linear Schrödinger equation (see Ref. 2 for a review of the exact treatment of DNLS). The Agranovich's theory is usually believed to capture the physics of nonlinear lattices when nonlinearity is a dominant feature. Indeed, a strong enough Hubbard interaction yields an isolated biphonon branch in the energy spectrum. The model drawback is that the energy terms that do not conserve the total boson number are neglected, although these terms stem from the potential energy of atoms and moreover they contribute significantly to the quantum hybridization. Consequently, the effective boson model gives a dispersion law which takes the form $(1 + C\cos(q))$ (with arbitrary units) instead of $\sqrt{1 + 2C\cos(q)}$, calculated in the simple harmonic approximation, with similar parameters (for details, see Sec. II). One notes that the two formula diverge with increasing the coupling coefficient C . Actually, according to Agranovich himself²¹, the effective Hubbard model for boson finds some substantiation in the work of F. Bogani³ where the author treated a lattice model similar to KG, i.e., derived from the realistic potential energy of molecules.

Further works could be realized on the basis of our numerics. The nonlinear lattices with a single-well onsite potential have been studied here. In some compounds, the energy landscape of atoms may involve more wells as for the H atoms in 4-methyl-pyridine (see Ref.24). The tunneling of quantum particles through the potential barriers is expected to change significantly the vibration spectrum. The study of a KG model with a multi-well onsite potential would permit to identify the specific features due to the onsite tunneling.

I gratefully acknowledge the financial supports from both the Trinity College (University of Cambridge, UK) and the Mathematics Institute (University of Warwick UK). The numerics was performed partly on the computers of the Department of Applied Mathematics and Theoretical Physics (University of Cambridge) and partly on the computers of the Service de Recherches de Métallurgie Physique (CEA/DEN/DMN, France). Many thanks are addressed to Robert S. MacKay and Serge Aubry for the enlightening discussions we had about the nonlinear lattices.

-
- ¹ V.M. Agranovich, *Spectroscopy and excitation dynamics of condensed molecular systems*, chp. 3, North-Holland publishing company (1983), pp. 83-138.
- ² J. C. Eilbeck, *Proceedings of the Third Conference Localization and Energy Transfer in Nonlinear Systems*, Eds. L. Vazquez, R. S. MacKay, M. P. Zorzano, World Scientific Singapore (2003), p.177.
- ³ F. Bogani, J. Phys. C: Solid State Phys. **11**, 1283 (1978).
- ⁴ V.M. Agranovich, Soviet Physics - Solid State **12**, 430 (1970).
- ⁵ F. Bogani, J. Phys. C: Solid State Phys. **11**, 1297 (1978).
- ⁶ W.Z. Wang, J.T. Gammel, A.R. Bishop and M.I. Salkola, Phys. Rev. Lett. **76**, 3598 (1996).
- ⁷ R.S. Mackay, Physica A **288**, 174 (2000).
- ⁸ V. Hizhnyakov, D. Nevedrov and A. J. Sievers , Physica B **316-317**, 132 (2002).
- ⁹ J. Dorignac and S. Flach, Phys. Rev. B **65**, 214305 (2002); V. Fleurov, R. Schilling and S. Flach, Phys. Rev. E **58**, 339 (1998).
- ¹⁰ V. Fleurov, Chaos **13**, 676 (2003).
- ¹¹ A. J. Sievers and S. Takeno, Phys. Rev. Lett. **61**, 970 (1988); S. Takeno, K. Kisoda and A. J. Sievers, Progress of Theoretical Physics Supplement **94**, 242 (1988).
- ¹² R.S. MacKay and S. Aubry, Nonlinearity **7**, 1623 (1994).
- ¹³ L.D. Landau and E. M. Lifshits, *Quantum Mechanics (Non-Relativistic Theory)*, Pergamon Press, New York (1965).
- ¹⁴ when $E_d = 0.1$ eV and $b = 2$ Å, the parameters in Eq. (8) are $A_3 = -0.09496$, $A_4 = 0.00451$ and $\hbar\Omega = 0.02886$ eV.
- ¹⁵ William H. Press, *Numerical Recipes in Fortran*, Cambridge University Press (1992), pp. 462-

475 ; <http://www.nr.com/> .

- ¹⁶ $\sqrt{2(w + \eta)} \rightarrow \Omega$ and $-\eta \rightarrow C.\Omega^2$, $v \rightarrow A_4.\Omega^3$ and $A_3 = 0$.
- ¹⁷ H. Mao and R.J. Hemley, Rev. Mod. Phys. **66**, 671 (1994).
- ¹⁸ P. Jakob, Phys. Rev. Lett. **77**, 4229 (1996); P. Jakob and B.N.J. Persson, J. Chem. Phys. **109**, 8641 (1998).
- ¹⁹ V. Pouthier, J. Chem. Phys. **118** 9364 (2003).
- ²⁰ V. Pouthier, J. Chem. Phys. **118** 9364 (2003); V. Pouthier, J. Chem. Phys. **118**, 3736 (2003); V. Pouthier and C. Falvo, Phys. Rev. E **69**, 041906 (2004).
- ²¹ V.M. Agranovich, *Spectroscopy and excitation dynamics of condensed molecular systems*, chp. 3, North-Holland publishing company (1983), p. 92.
- ²² Morrel H. Cohen and J. Ruvalds, Phys. Rev. Lett. **23**, 1378 (1969).
- ²³ R. Tubino and J. L. Birman, Phys. Rev. Lett. **35**, 670 (1975).
- ²⁴ F. Fillaux *et al.*, Phys. Rev. B **68**, 224301 (2003)

Table caption

Tab. I: Values of the bracket $(2 < \phi_{\alpha,i}|X_i|\phi_{0,i} >^2)$ for different α and different nonlinear parameters, A_3 and A_4 , used in computations of Figs. 5-11.

Figure captions

Fig. 1: Energy spectrum of a single *He* atom embedded into a double-well potential. (a) The semi-classical calculation (square symbols, dashed line) is compared to the Hamiltonian diagonalization (circle symbols, solid line) onto the truncated Einstein basis with a frequency $\omega_0 = \sqrt{32.E_0/(mb^2)}$. The insert shows the double-well plot versus the displacement (in Å). (b) The later method is shown to converge when the basis cutoff N increases.

Fig. 2: Plot of the bracket $\langle \phi_{\alpha,i} | X_i | \phi_{0,i} \rangle$ for the nonlinear parameters $A_4 = 0.2$ and $A_3 = 0$ (solid line with triangle symbols) and $A_4 = 0.01$ and $A_3 = 0.13$ (dashed line with circle symbols)

Fig. 3: (color online) For a unitless coupling $C = 0.1$, comparison between the analytical calculation (dark solid line) and our numerics (see in Sec. II), for the Hamiltonian eigenvalues of a 1D harmonic chain, composed of $S = 25$ atoms. The energy-spectrum is arranged in increasing order and it is measured with respect to the groundstate. The numerics are performed for different upper number of onsite excitations $N_{cut} = 4$ (blue solid line, circle symbols), $N_{cut} = 3$ (red dotted line, squares) and $N_{cut} = 2$ (green dot-dashed line, triangles).

Fig. 4: Eigen-spectrum of a 4 sites 1D lattice with a Φ^4 onsite potential. Model parameters are given in Ref. 16. Comparison between our numerics (circle symbols) and Ref. 6 (diamond symbols) (see Sec. II). The Y-axis unit is $\hbar\Omega$ and its zero is the groundstate energy. On the X-axis, the lattice first Brillouin zone is reported.

Fig. 5: Plots of the energy branches of a 1D chain, composed of $S = 33$ atoms, for $C = 0.05$, $A_3 = 0$ and $A_4 = 0.2$ in (a) and for $C = 0.05$, $A_3 = 0$ and $A_4 = 0.02$ in (b). The left insert shows a magnification of the fundamental branch while the overtone region is magnified in the right insert. The biphonon branch is marked by $(\{2\})$ and the two-phonon band by $(\{11\})$. The same tags point into the insert. The Y-axis unit is $\hbar\Omega$ and its zero is the groundstate.

Fig. 6: Same as Fig. 5 but for different nonlinear parameters, i.e., $A_4 = 0.01$ and

$A_3 = 0.13$ in (a) and $A_4 = 0.01$ and $A_3 = 0.105$ in (b).

Fig. 7: Versus the unitless coupling C , plot of the energy spectrum of a 1D chain, composed of $S = 19$ atoms for $A_4 = 0.2, A_3 = 0$. in (a) and for $A_4 = 0.01, A_3 = 0.13$ in (b). The tags are explained in the text.

Fig. 8: (color online) On the left hand side, energy spectrum of a 2D square lattice in the region of the biphonon for $C = 0.025, A_3 = 0$ and $A_4 = 0.1$ (top) and for same parameters but $A_4 = 0.025$ (bottom). The lattice size is $S = 13 \times 13$ atoms. On the right hand side, profiles of the left-hand side spectra along the direction $[11]$. The inserts show the magnification of the phonon branch and the biphonon energy region.

Fig. 9: (color online) Versus the unitless distance n , plot of the correlation functions $f(\Phi, n)$ for 3 eigenstates of a 1D lattice which size is $S = 23$. Parameters are $A_4 = 0.2, A_3 = 0, C = 0.05$. The eigenstates correspond to the phonon states (a), the biphonon (b) and the triphonon (c) with for each of them different wave vectors $q = 0$ (circles), $q = 4\pi/S$ (triangles), $q = 10\pi/S$ (diamonds), $q = 16\pi/S$ (squares) and $q = 22\pi/S$ (triangles). The inserts in Fig. (b) and (c) show a magnification of the zero y-axis.

Fig.10: (color online) Same as Fig. 9 but for $A_4 = 0.01, A_3 = 0.13$ and $C = 0.05$.

Fig. 11: (color online) Same as Fig. 9 but for two eigenstates for parameters $A_4 = 0.02, A_3 = 0$. and $C = 0.05$. The eigenstates correspond to the phonon states (a) and the biphonon (b).

Fig.12: Versus the unitless parameter A_4 , plot of the scalar product $|\langle \psi_\alpha(q) | \Phi_\alpha(q) \rangle|^2$ (see Sec. IV) for $C = 0.05$ and $A_3 = 0$ and for $q = 0$ (solid lines) and $q = \pi$ (dashed lines). The eigenstates correspond to the phonon states $\alpha = 1$ (a), the biphonon states $\alpha = 2$ (b), and the triphonon states $\alpha = 3$ (c).

$2 < \phi_{\alpha_i} X_i \phi_{0_i} >^2$	$A_4 = 0.2 \ A_3 = 0$ Fig.5(a) & Fig.9	$A_4 = 0.01 \ A_3 = 0.13$ Fig.6(a) & Fig.10	$A_4 = 0.02 \ A_3 = 0$ Fig.5(b) & Fig.11	$A_4 = 0.01 \ A_3 = 0.105$ Fig.6(b)
$\alpha = 1$	0.74	1.06	0.95	1.03
$\alpha = 2$	0.	2.9710^{-2}	0.	1.1610^{-2}
$\alpha = 3$	7.3910^{-4}	2.3610^{-3}	7.910^{-5}	3.310^{-4}
$\alpha = 4$	0.	3.9110^{-4}	0.	1.0910^{-5}
$\alpha = 5$	8.4510^{-7}	5.4510^{-5}	1.4510^{-8}	4.3910^{-7}

TABLE I: (2004) L. Proville

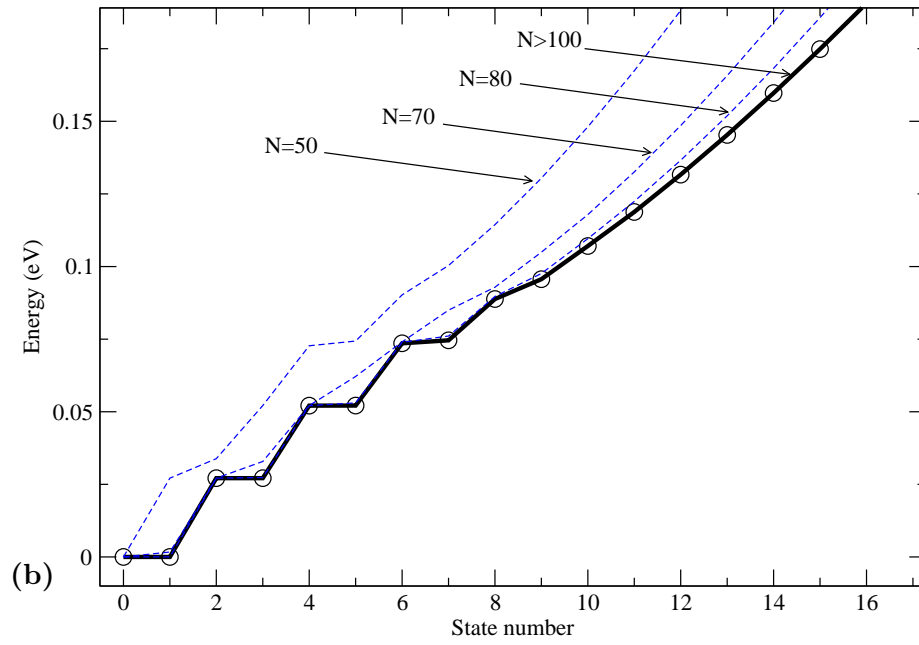
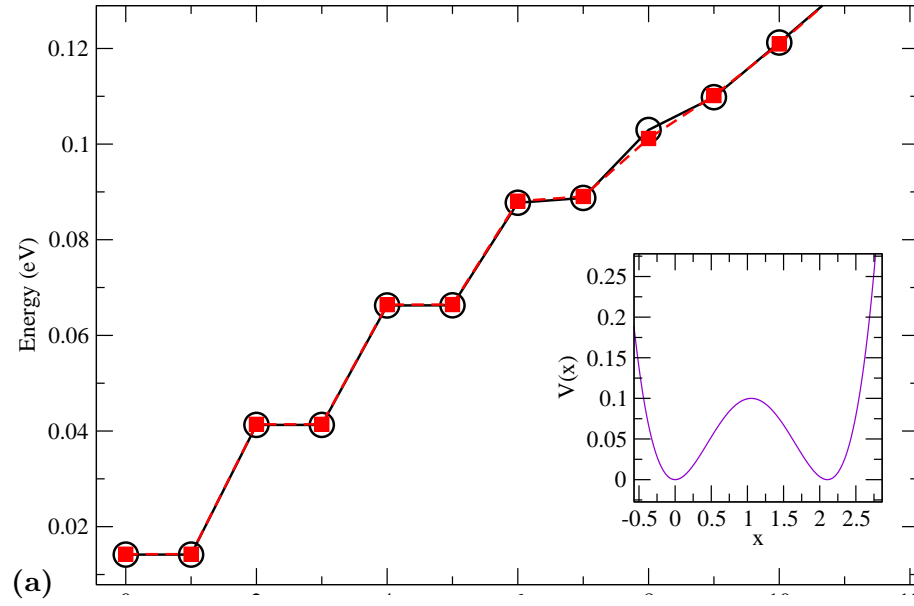


FIG. 1: (2004) L. Proville

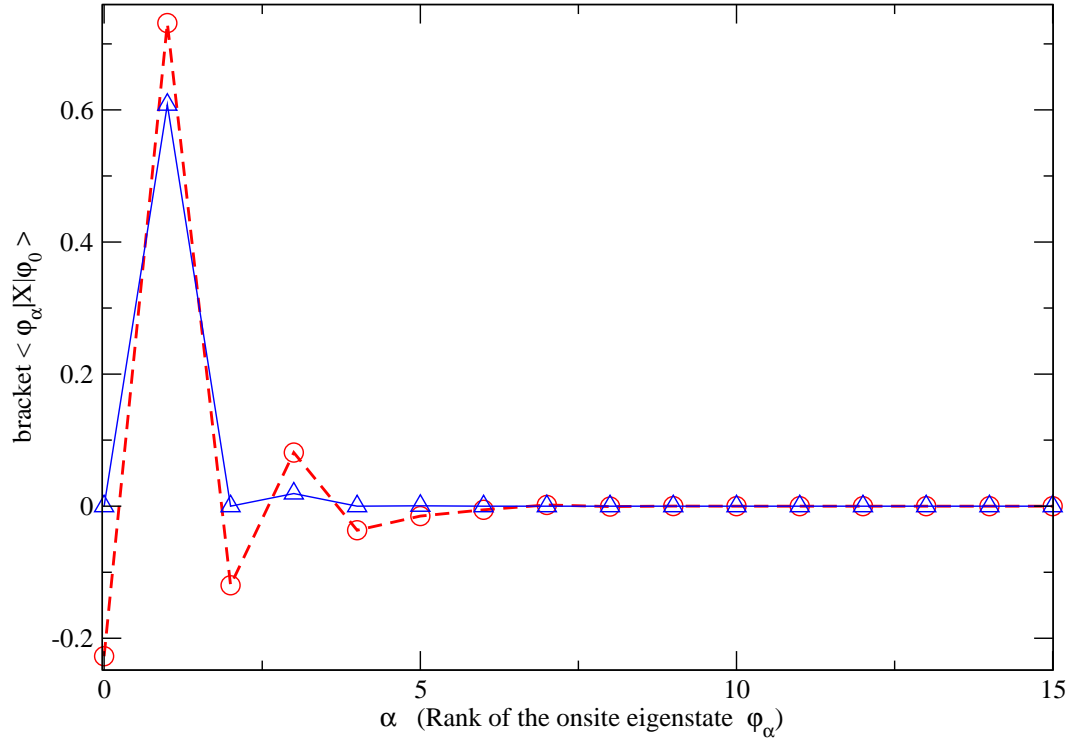


FIG. 2: (2004) L. Proville

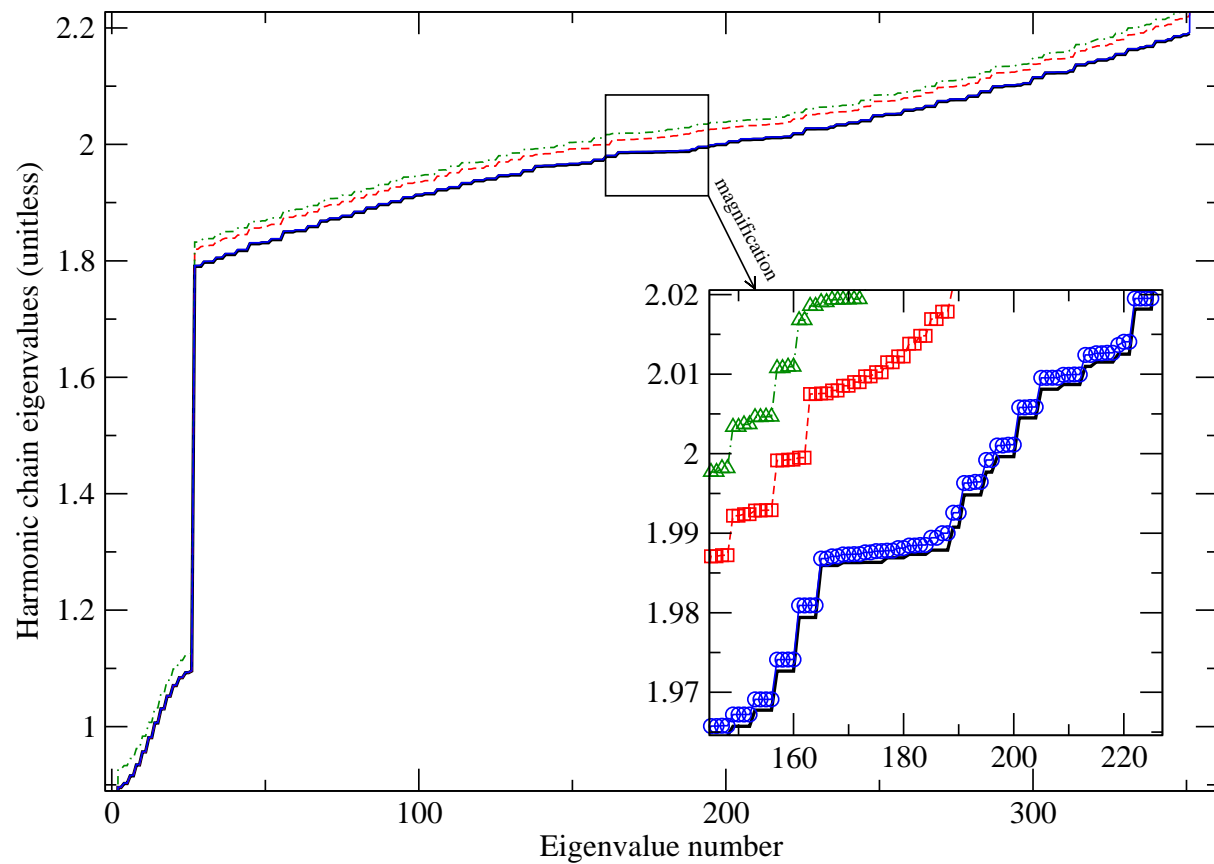


FIG. 3: (2004) L. Proville

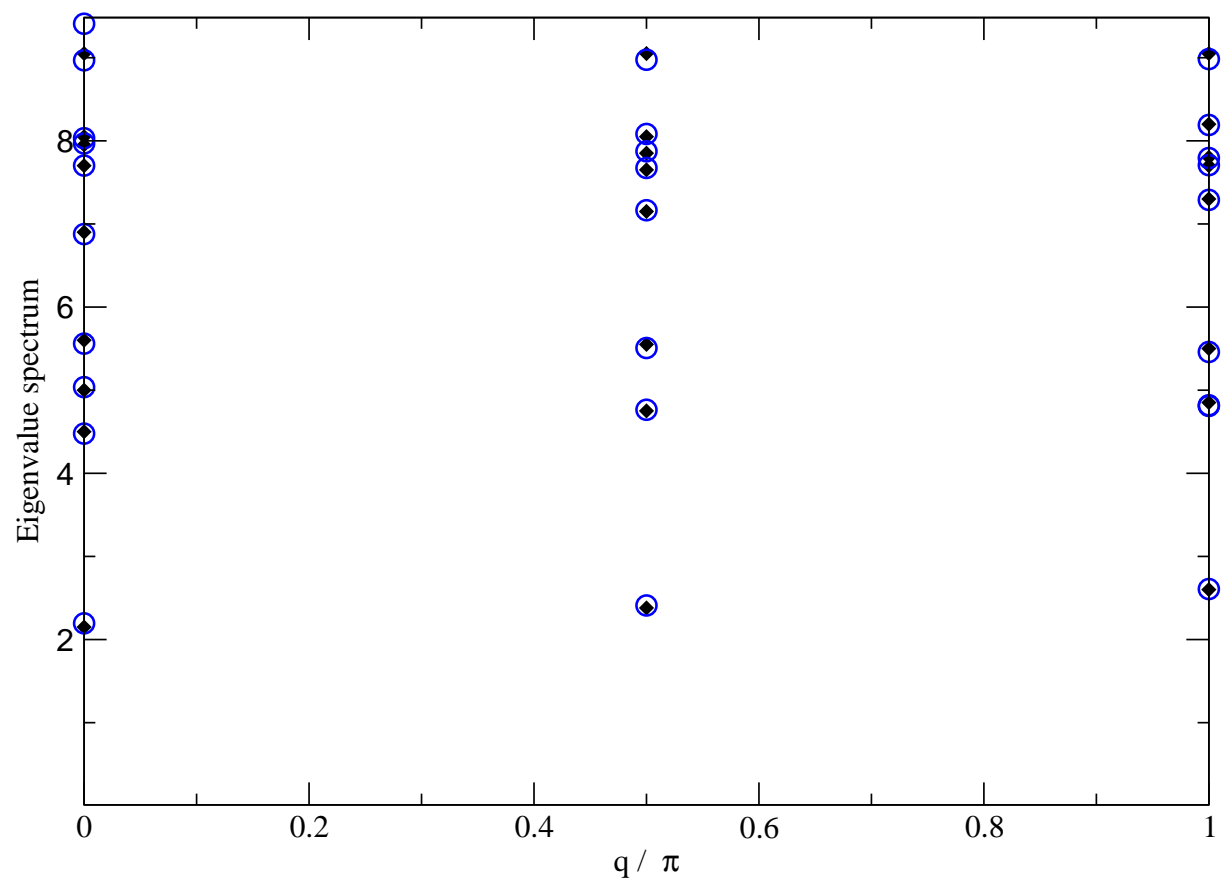


FIG. 4: (2004) L. Proville

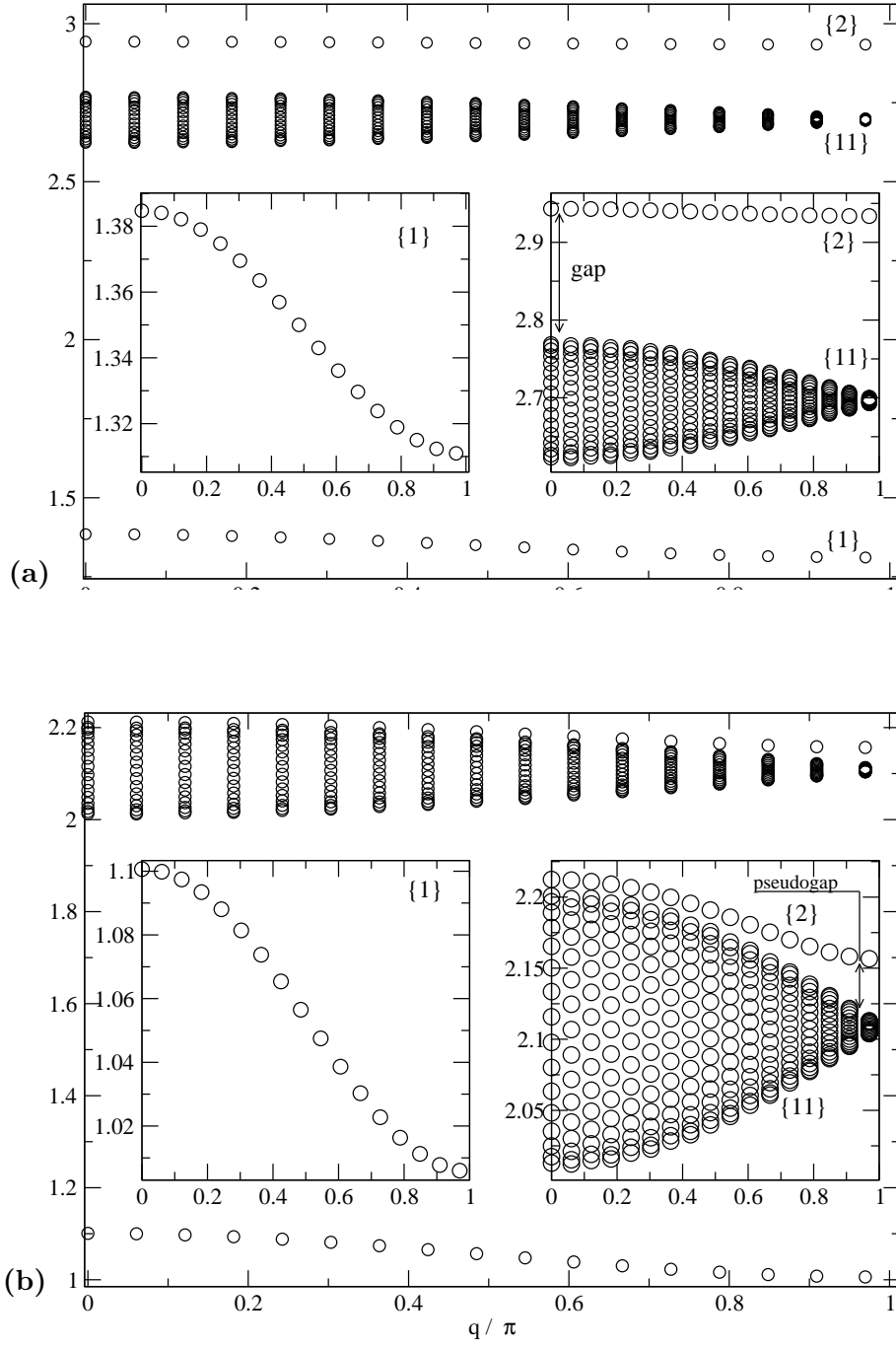


FIG. 5: (2004) L. Proville

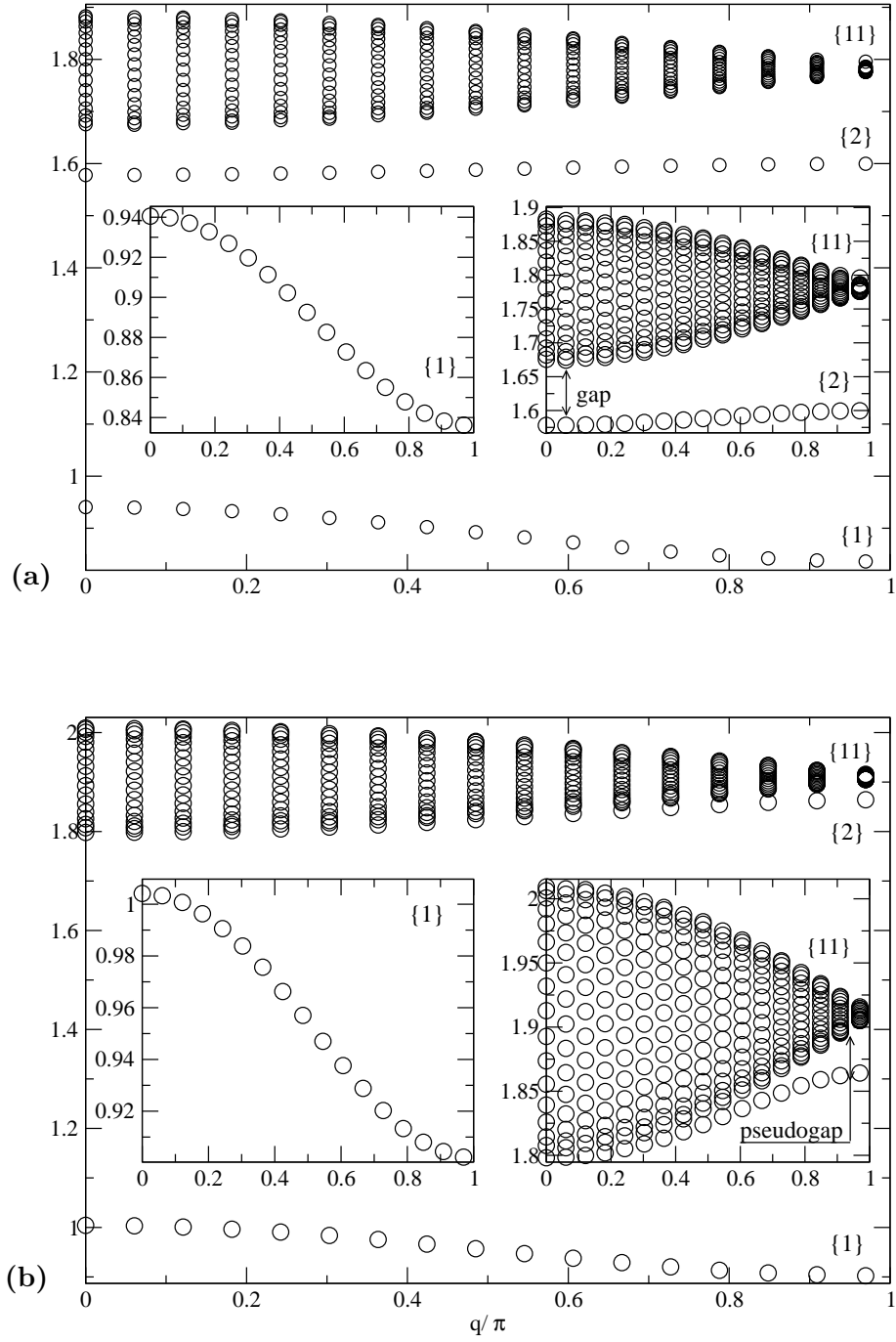


FIG. 6: (2004) L. Proville

(b)

FIG. 7: (2004) L. Proville (See PNG formatted figures)

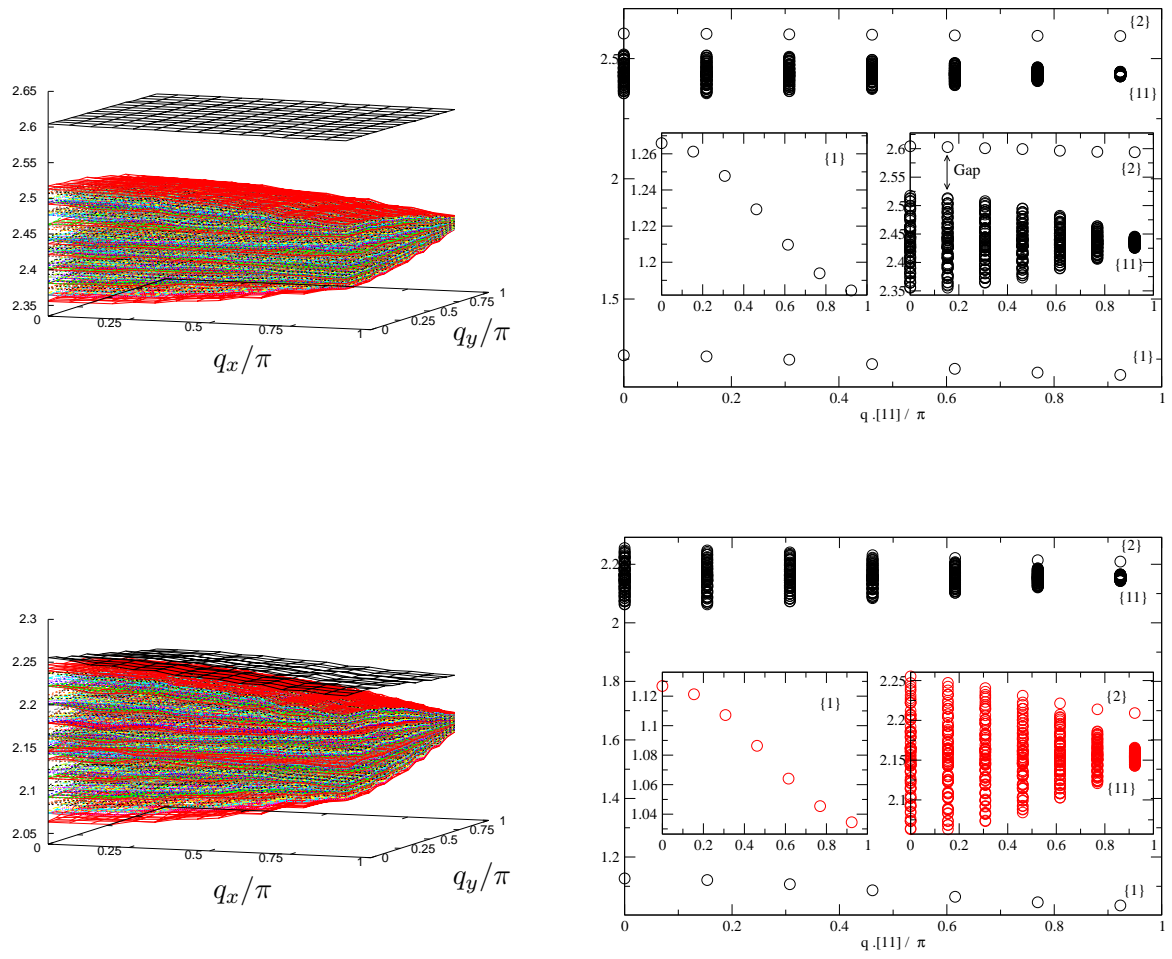
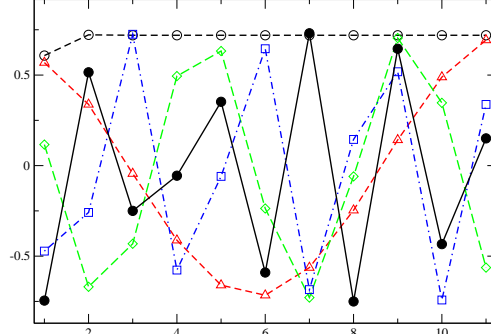
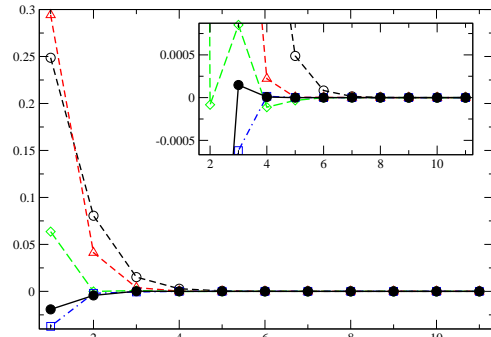


FIG. 8: (2004) L. Provile

(a)



(b)



(c)

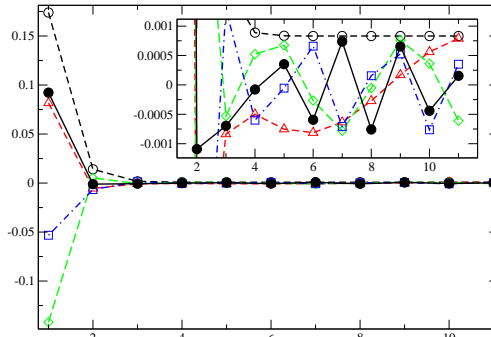


FIG. 9: (2004) L. Proville

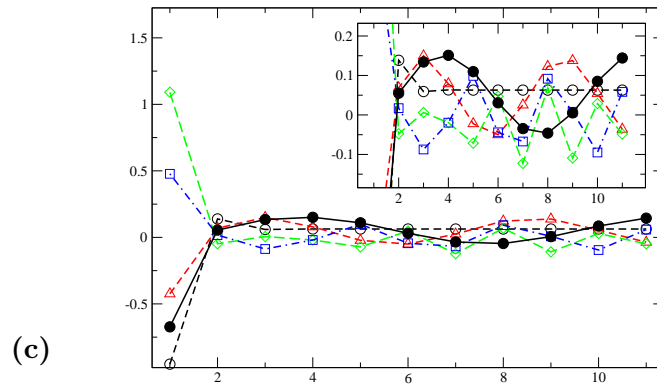
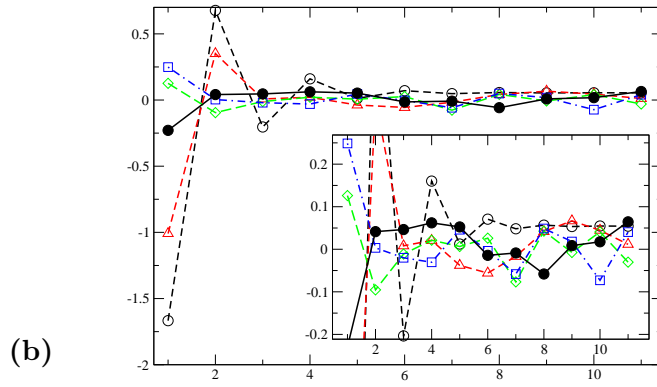
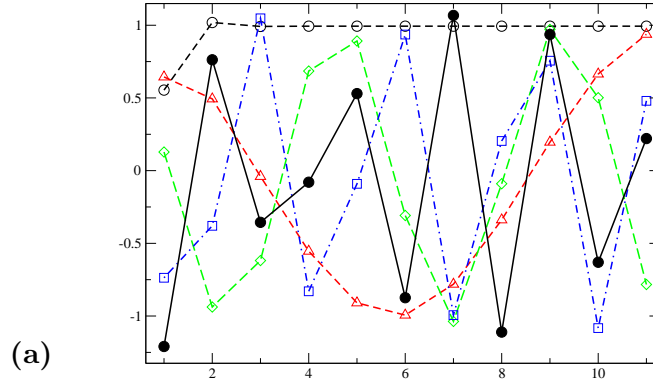


FIG. 10: (2004) L. Proville

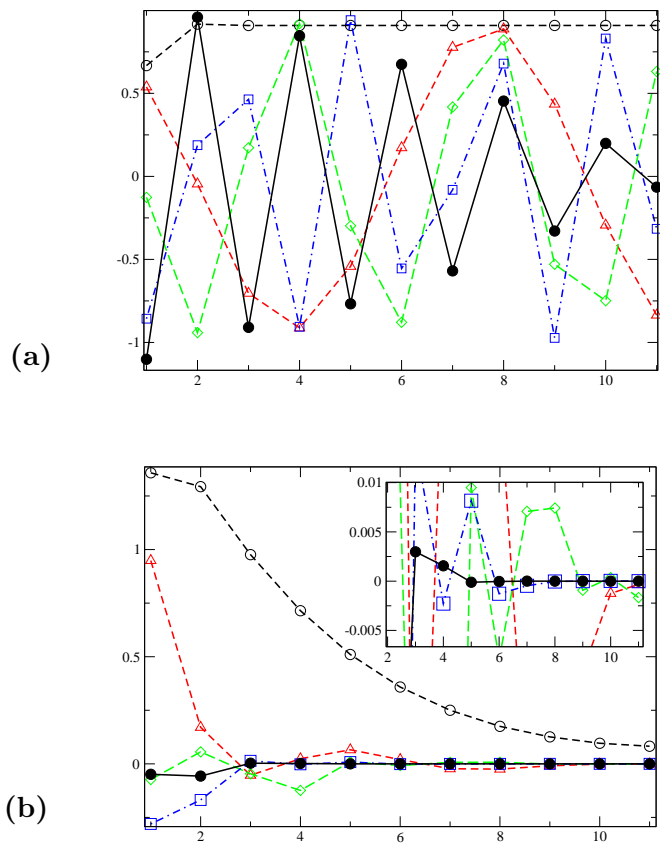


FIG. 11: (2004) L. Proville

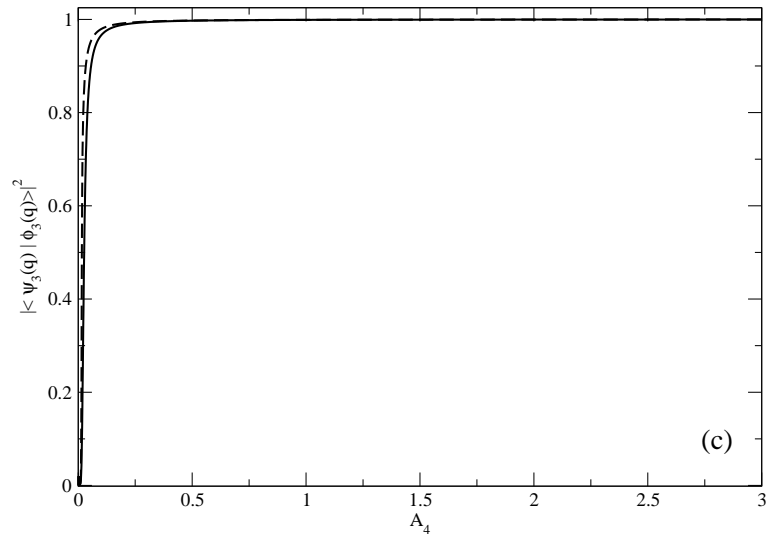
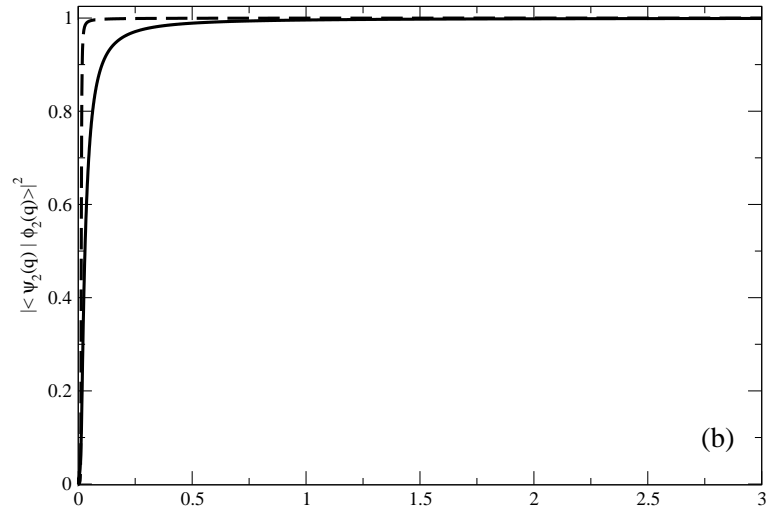
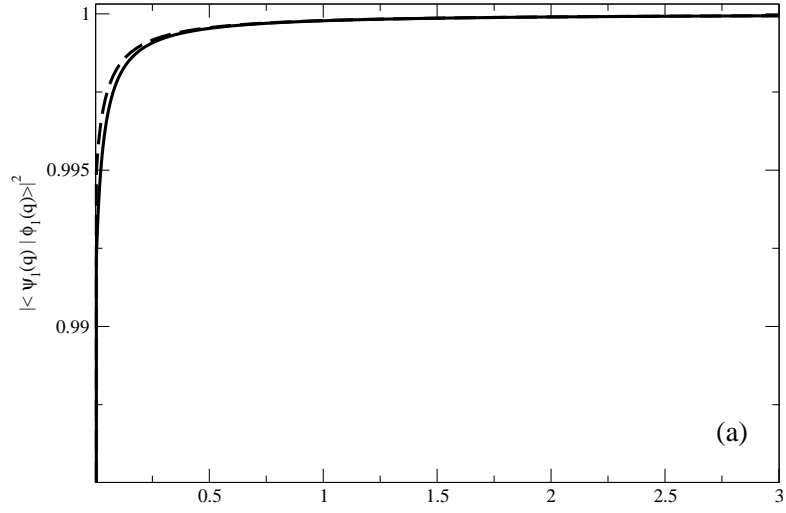


FIG. 12: (2004) L. Proville

This figure "fig7aPROVILLE.png" is available in "png" format from:

<http://arxiv.org/ps/cond-mat/0403516v5>

This figure "fig7bPROVILLE.png" is available in "png" format from:

<http://arxiv.org/ps/cond-mat/0403516v5>